Convex Hull Approach for Determining Rock Representative Elementary Volume for Multiple Petrophysical Parameters using Pore-scale Imaging and Lattice-Boltzmann modelling.

S.M.Shah*, F.Gray, J.Yang, J.P.Crawshaw, and E.S.Boek

Qatar Carbonates and Carbon Storage Research Centre (QCCSRC)
Department of Chemical Engineering, Imperial College London, London SW7 2AZ, UK

Corresponding author: *Saurabh M Shah (saurabh.shah10@imperial.ac.uk)

Highlights

- Qualitative and quantitative method to capture heterogeneity at pore-scale
- Multiple petrophysical parameters to determine Representative Element Volume
- Enhancing computational efficiency to calculate petrophysical properties

Abstract

In the last decade, the study of fluid flow in porous media has developed considerably due to the combination of X-ray Micro Computed Tomography (micro-CT) and advances in computational methods for solving complex fluid flow equations directly or indirectly on reconstructed three-dimensional pore space images. In this study, we calculate porosity and single phase permeability using micro-CT imaging and Lattice Boltzmann (LB) simulations for 8 different porous media: beadpacks (with bead sizes 50μm and 350 μm), sandpacks (LV60 and HST95), sandstones (Berea, Clashach and Doddington) and a carbonate (Ketton). Combining the observed porosity and calculated single phase permeability, we shed new light on the existence and size of the Representative Element of Volume (REV) capturing the different scales of heterogeneity from the pore-scale imaging. Our study applies the concept of the 'Convex Hull' to calculate the REV by considering the two main macroscopic petrophysical parameters, porosity and single phase permeability, simultaneously. The shape of the hull can be used to identify strong correlation between the parameters or greatly differing convergence rates. To further enhance computational efficiency we note that the area of the convex hull (for well-chosen parameters such as the log of the permeability and the porosity) decays exponentially with sub-sample size so that only a few small simulations are needed to determine the system size needed to calculate the parameters to high accuracy (small convex hull area). Finally we propose using a characteristic length such as the pore size to choose an efficient absolute voxel size for the numerical rock.

Keywords

Representative Element Volume, porosity, single phase permeability, pore-scale, convex hull

1. Introduction

The physics of fluid flow through complex porous media has important applications in petroleum and reservoir engineering, including the displacement of oil, gas and water in hydrocarbon reservoirs and is of particular interest to understand the trapping of CO_2 for carbon storage applications (Fredrich, 1999; Andrew, Bijeljic, & Blunt, 2013; Shah, Yang, Crawshaw, Gharbi, & Boek, 2013). In the past, many researchers have attempted to relate fluid transport properties such as permeability to the bulk porosity and specific surface area, but complexity arises in predicting permeability accurately (Bear, 1972; Walsh & Brace, 1984; Mostaghimi, Blunt, & Branko, 2013). Fluid transport properties depend critically on the size, shape and connectivity of the pore space and geometry of the porous medium. However, there is no accurate formula which can correlate permeability with bulk porosity without ambiguity. This motivated research in pore-scale imaging and modelling to obtain detailed information about the geometry of complex porous media and modelling the fluid flow at the pore-scale using different numerical simulation methods to predict the permeability accurately (Blunt, Jackson, Piri, & Valvatne, 2002; Valvatne & Blunt, 2004; Dong & Blunt, 2009; Boek & Venturoli, 2010; Yang, Crawshaw, & Boek, 2013; Shah, Crawshaw, & Boek, 2016). Pore-scale imaging and modelling is developing quickly and has now become a routine service in the petroleum industry, principally to understand displacement processes and to predict single phase and relative permeability (Blunt, et al., 2013). The fundamental problem in pore-scale imaging and modelling is how to represent and model the different range of scales encountered in porous media, starting from the unresolved sub-resolution micro-porosity. Bear [1972] has explained the concept of Representative Element of Volume (REV), qualitatively taking into consideration a macroscopic property, such as porosity. The REV is the minimum volume that can represent a particular macroscopic property of the sample. Figure (1) shows a graph to define the REV, where ΔU_i is defined as a volume in a porous medium, and is considered to be much larger than a single pore or grain. ΔU_v is the volume of void space, and the fractional porosity is defined by n_i, as the ratio of void space to volume. As shown in Figure (1), there are minimal fluctuations of porosity as a function of volume at large values of ΔU_i. As the volume decreases, fluctuations in the porosity increase, specifically as ΔU_i approaches the size of a single pore, which has a fractional porosity of 1. Therefore the REV is defined by the term ΔU_0, above which fluctuations of porosity are minimal, and below which fluctuations of porosity are significant. The determination of the volume ΔU_i is related to the different length scales varying from pore-scale to core scale to continuum scale (Crawshaw & Boek, 2013).

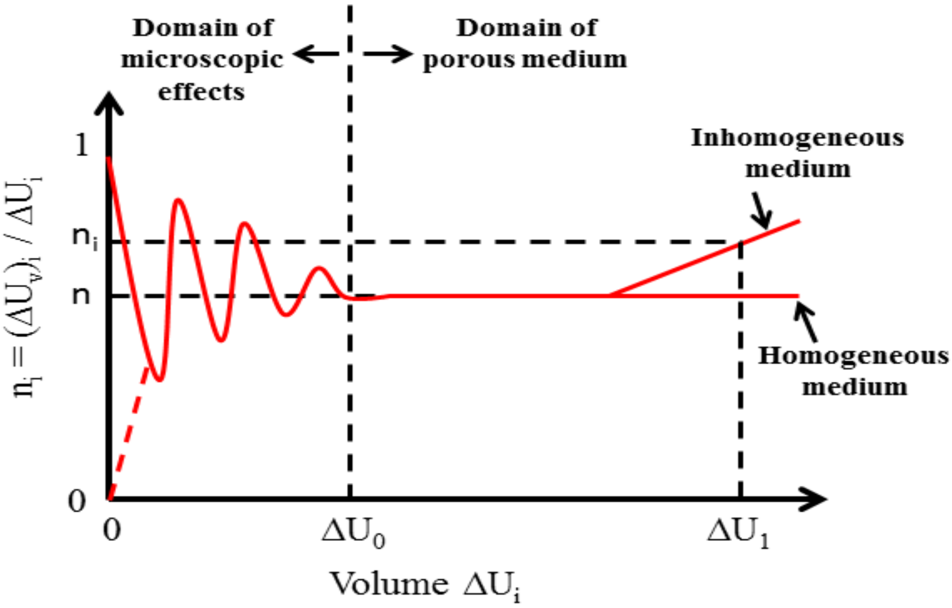

Figure 1 Schematic diagram showing the measured property varies with the sample volume and the domain of the Representative Element Volume (REV) (Crawshaw & Boek, 2013).

Pore-scale techniques have to answer questions such as: "What is the actual size of an REV? Does the size of the REV vary for different rock types? Are the REVs similar or significantly different for different quantities at a given location? How do the transport and structural properties such as permeability and porosity vary with scale?" (Zhang, Zhang, Chen, & Soll, 2000). The above listed questions were partly answered by Bear [1972], Bosl et al. [1998], Pan et al. [2001], Zhang et al. [2000], Keehm [2003], Peng et al. [2012], Peng et al. [2014] and Mostaghimi et al. [2013].

Two types of numerical method for assessing the size of an REV are commonly used. The first is the "deterministic REV", in this scheme, a sub-sample centred within a larger domain is gradually expanded. When the variation of petrophysical properties with sample size becomes small enough, REV size is considered to have been reached. Zhang et al. (2000) used this approach to compare results obtained from crushed glass beads and sandstone, and found that the size of an REV varies spatially and depends on the quantity being represented. Keehm [2003] found that to predict the absolute and relative permeability of porous media, a minimum REV of size $L = 20a$ is needed, where a is the mean pore size of the porous medium using analysis of 2D thin sections. Mostaghimi et al. [2013] demonstrated that the REV for permeability is larger than for static properties, such as porosity and specific surface area. They also found that the REV for carbonate rocks appears to be larger than the image size considered. The alternative approach is the "statistical REV" in which a number of sub-volumes at a given size are sampled over a larger domain. The width of the distribution of a given property decreases with increasing sub-sample sizes and can be used to define an REV below a certain threshold (Al-Raoush & Papadopoulos, 2010). However these previous studies only partly address issues regarding the concept of REV for pore-scale imaging and modelling and show its limitations. In this study we will address the correlation of REV with pore size and introduce a method by which the REV can be established for multiple parameters, considering porosity and permeability as an example.

We will now discuss the concepts of homogeneity and heterogeneity related to porous media studies. Homogeneity is defined qualitatively as the characteristic that a physical property has the same value in different elemental volumes regardless of their location (Olea, 1991). Therefore, the terms heterogeneity and homogeneity are dependent on the model or sample volume of the measured physical property (Nordahl & Ringrose, 2008). In this study, we systematically investigate the relation between two important macroscopic properties, porosity and absolute permeability, using pore-scale imaging and modelling techniques, to predict the representative element volume (REV). We use the mathematical concept of the Convex Hull, C_H to investigate the relation between porosity and permeability and examine the effects of rock sample heterogeneity and increasing sample size. The main aim is to explore this relation for 8 different types of porous materials, ranging from beadpacks to sandpacks to sandstones to carbonate rocks in terms of increasing heterogeneity and quantitatively determine the size of the REV for each. The approach could be extended to more complex flow calculations in porous media such as two-phase relative permeability and capillary pressure prediction.

2. Pore-scale Imaging and Modelling

The problem of REV determination in porous media can be quantitatively addressed using X-ray micro computed tomography (micro-CT), which is a widely used 3D imaging technique to obtain 3D images of porous media (Zhang, Zhang, Chen, & Soll, 2000). In addition, we use recent advances in computational methods for solving flow equations in complex geometries (Blunt, Jackson, Piri, & Valvatne, 2002; Blunt, et al., 2013; Boek & Venturoli, 2010; Yang & Boek, 2013). Pore-scale images of the rocks can be obtained using micro-CT equipment using laboratory and synchrotron sources. Spanne et al. [1994] and Auzerais et al. [1996] used micro-CT to obtain 3D voxel data of sandstone at a voxel resolution of around 7.5µm. Blunt et al. (2013) have obtained data for carbonate samples at different voxel resolutions ranging from 2.68µm to 13.7µm. The reconstructed pore geometries from micro-CT have been used for the prediction of petrophysical properties including permeability, porosity and formation factor (Arns, Knackstedt, Pinczewski, & Martys, 2004; Knackstedt, et al., 2006; Shah, Crawshaw, & Boek, Micro-Computed Tomography Pore-scale Study of Flow in Porous Media:Effect of Voxel Resolution, 2016).

In this study, we compute absolute permeability using the Lattice Boltzmann (LB) method. This model is particularly suited to direct numerical simulation on pore-space images because of its ability to handle complex boundaries accurately. Moreover, the LB method does not require extracting a simplified network of flow paths, as in network modelling (Zhang, Zhang, Chen, & Soll, 2000), and so is able to give accurate permeability results in highly heterogeneous media. The LB model describes the fluid as a velocity distribution of particle distribution function at each node. These undergo streaming and collision steps according to a discrete form of the Boltzmann equation, and can be shown to recover the incompressible Navier-Stokes equations (Chen, Wang, Shan, & Doolen, 1992). The single-phase D3Q19 lattice Boltzmann (LB) model with a multiple-relaxation-time (MRT) operator is used in our code (Yang, Crawshaw, & Boek, 2013).

3. Methods and Techniques

The detailed 3D micro-CT image acquisition procedure is presented by Shah et al. [2015]. Figure 2 shows 2D cross sections of 3D voxel data for 8 different porous materials, including beadpacks of two different bead sizes, two sandpacks, three sandstones and one carbonate. The 3D images for all the samples were subsequently segmented into binary images based on a 2D histogram segmentation analysis by using marker seeded watershed algorithm within the program Avizo Fire 8.0 (Visual Sciences Group, Burlington, MA, USA) (Shah, Crawshaw, & Boek, Micro-Computed Tomography Pore-scale Study of Flow in Porous Media:Effect of Voxel Resolution, 2016). 3D images of beadpacks, sandpacks, sandstones and carbonate samples were first cropped into 3D cubic images. The exact image dimensions, properties and details are summarized in Table 1.

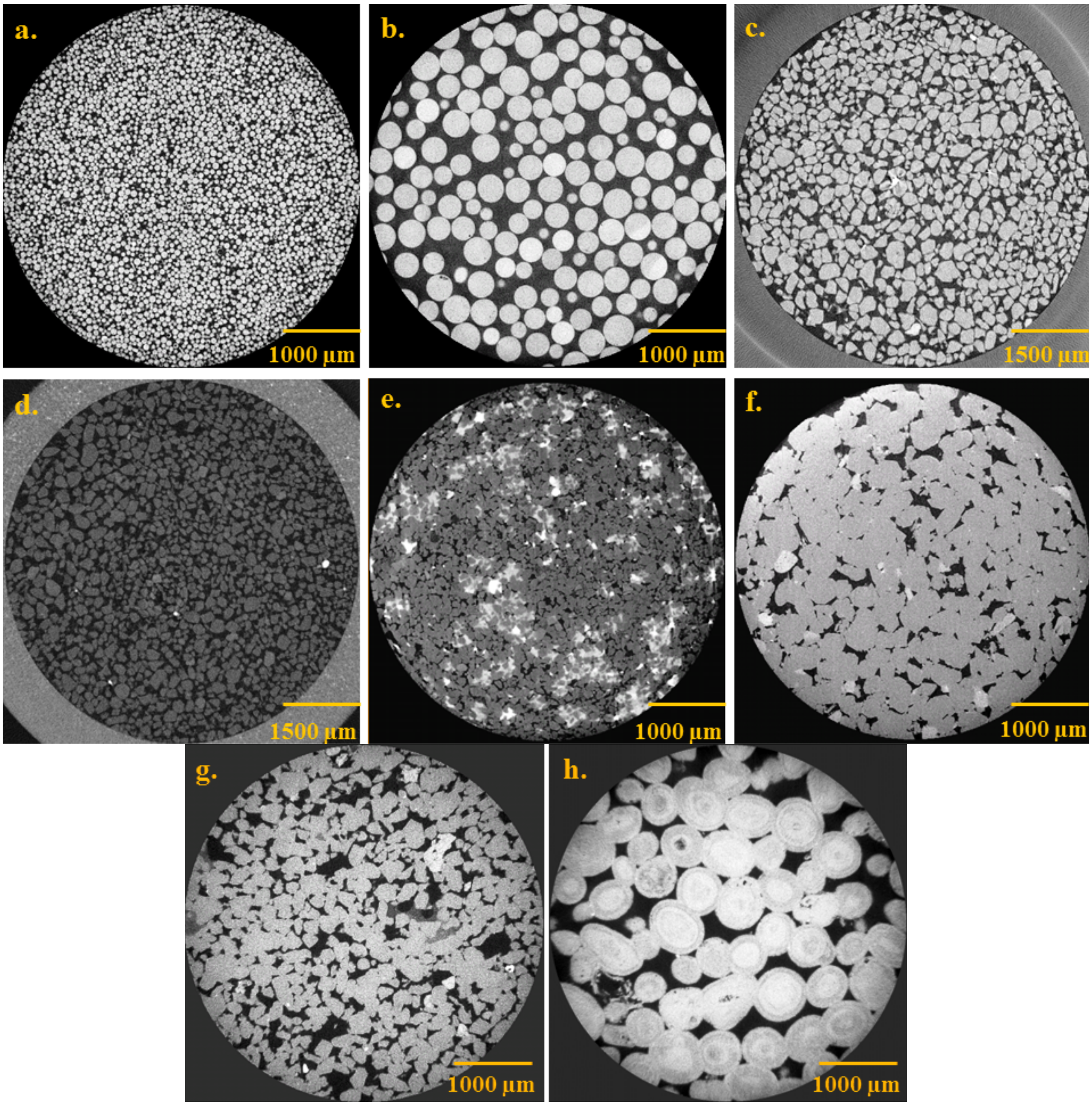

Figure 2 Two-dimensional cross sections of three dimensional micro-CT images of different samples. (a) Beadpack with grain size 50 µm. (b) Beadpack with grain size 350 µm. (c) LV60 sandpack (d) HST95 sandpack (e) Berea sandstone (f) Clashach sandstone (g) Doddington sandstone (h) Ketton carbonate. In all figures, the pore space is shown in dark.

Table 1: Summary of the rocks and images studied in this paper. Porosity and single phase permeability obtained from computation.

Sample	Source/ Scanner	Image Size, Voxels	Voxel Size (µm)	Porosity[†] (%)	Single Phase Permeability[†] (mD)
Beadpack -50 µm	Micro-CT	700^3	4.21	28.5	1474
Beadpack- 350 µm[a]	Synchrotron	700^3	5.35	36.40	95400
LV60 sandpack[b]	Micro-CT	400^3	7.24	30.55	11860
HST95 sandpack[b]	Micro-CT	400^3	7.89	30.27	5235
Berea sandstone	Micro-CT	700^3	4.52	9.52	58
Clashach sandstone	Micro-CT	700^3	4.52	10.78	448
Doddington sandstone	Micro-CT	700^3	4.52	16.35	2442
Ketton carbonate	Micro-CT	700^3	4.52	13.04	5648

[†] Computed from the destined voxels using Lattice Boltzmann code
[a] Data obtained from Kamaljit Singh through personal communication
[b] (Dong & Blunt, 2009)

The properties predicted from the images depend on the segmented pore space adequately representing the voids in the rock sample. This becomes problematic when a significant fraction of the porosity contributing to flow is below the resolution of the micro-CT image, as can be the case for many carbonate rocks (Grey, Cen, Shah, Crawshaw and Boek 2016). In the Ketton carbonate used here, the segmented pore space image was well connected and micro-porous regions were assigned to the solid phase without compromising the subsequent flow simulations.

The experimental (total) porosity and single-phase permeability were measured on each of the cylindrical core samples except beadpacks and sandpacks. The total porosity was measured using bulk volume measurements and single phase permeability was measured using the Darcy flow equation. Brine was injected at constant flow rate and the pressure drop across the length of the sample was monitored using a high precision pressure transducer. A flow cell was designed to accurately measure the single phase permeability of the core samples at three different flow rates (Gharbi & Blunt, 2012). Note that these measurements are for the whole sample volume and not only the scanned region. The experimental porosity and single phase permeability of each sample are presented in Table 2.

Samples	Length [mm]	Diameter [mm]	Experimental Porosity [%]	Experimental Permeability [mD]
LV60 sandpack**	-	-	37.00 ±0.2	32000 ±300
HST95 sandpack**	-	-	33.4	7900
Berea sandstone	15.2	5	11.17 ±0.4	17.5 ±0.7
Clashach sandstone	11.6	5	11.02 ±0.2	365 ±116
Doddington sandstone	17.8	6	18.41 ±0.5	2362 ±221
Ketton carbonate	15.1	5	19.02 ±0.1	4271 ±300

Table 2: Experimental petrophysical properties of the rocks considered in the present study

**Experimental porosity was measured on a packed column using bulk volume measurement and experimental brine permeability was measured on a packed column by injecting brine at a constant flowrate (Pentland, 2010).

The pore geometries of the porous samples are partitioned into several sub-domains which are of the same size (Figure 3). For example, we consider 3D micro-CT data of a Doddington sandstone sample consisting of 700^3 voxels with 4.5μm voxel resolution representing a physical area of 3.15 mm. We then perform this subsampling procedure with each of the 6 sub-domain sizes given in Table 3. The division of the geometry into different voxels or image sizes is done in x-, y- and z- directions. The statistical distribution of parameters obtained from individual subsamples allows for the characterisation of the sample REV.

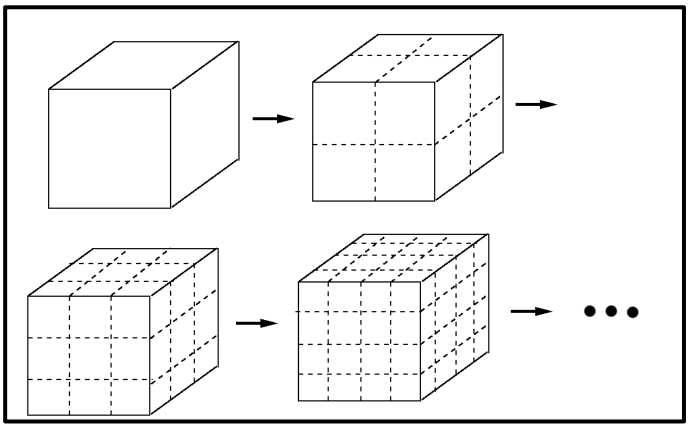

Figure 3 An example of domain partition. The scanned sample was divided into n^3 sub-domains which have the same size.

For the LB flow simulation, we impose a body-force throughout the domain or sub-domain and periodic boundary conditions at the inlet and outlet faces, iterating the flow-field until it reaches steady-state. Then, the single phase permeability is obtained from Darcy's law. For smaller sub-domains, there is no guarantee of convergence of the velocity field to steady-state. This is either because there is no flow path percolating between flow faces, or because there is too little solid phase. In these cases, the simulation continues for up to 50,000 LB time-steps. The sub-volume is discounted if the velocity field does not converge by this limit. The calculation was run on a Tesla K20 GPU with a 5GB memory but in cases where the sub-volume calculation required more memory than this, the calculation was deferred to CPUs. The calculated LB single phase permeability varies significantly for sub-domains therefore we normalise the permeability independently for each porous sample by $k' = \frac{k_{sub-domain}}{k_{total}}$ where $k_{sub\text{-}domain}$ is the calculated LB permeability of the particular single sub-domain size [mD], k_{total} is the calculated LB permeability of the whole domain (700^3 voxel) [mD] and k' is the normalised dimensionless permeability.

Table 3 Division of sub-domain voxel size from the whole domain of 700^3 with calculated linear dimensions from the voxel resolution for Doddington sandstone sample.

Doddington sandstone Resolution – 4.5μm	Sub-domain 700^3 voxels	Linear dimension [μm]
1	50 x 50 x 50	225
2	100 x 100 x 100	450
3	150 x 150 x 150	650
4	200 x 200 x 200	900
5	250 x 250 x 250	1125
6	300 x 300 x 300	1350
7	350 x 350 x 350	1575

4. Results and Discussion

The porosity and single phase permeability for each sub-domain is calculated and used to obtain the 'Convex Hull' for that domain size. The concept of the convex hull was explained by Andrew (1979). Let us imagine the points S as being pegs; the convex hull of S is the shape of a rubber band stretched around the pegs. The formal way to define the convex hull of S is the smallest convex polygon that contains all the points of S as shown in figure 4.

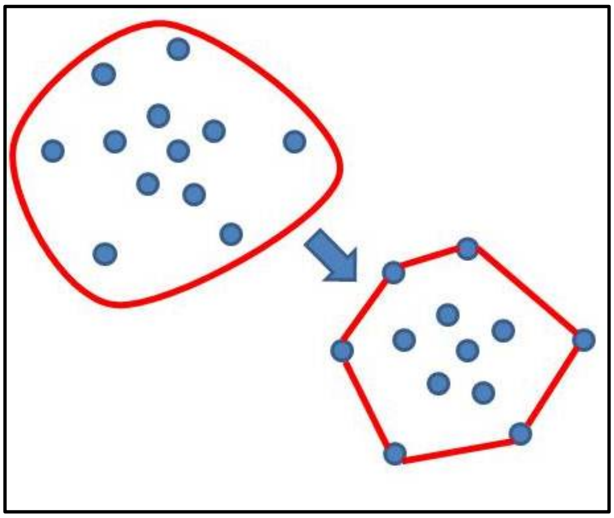

Figure 4. Example explaining the definition of convex hull of set of points S.

The process of obtaining a convex hull for each sub-domain was repeated for each of the 7 samples. Figure (5) shows the calculated porosity and single-phase permeability together with the corresponding convex hulls for Doddington sandstone, for different sub-domains varying from 50^3 to 350^3 voxels. Next we calculate the area of the resulting convex hulls and plot these against the domain size in voxels, shown in Figure 6 for all the samples.

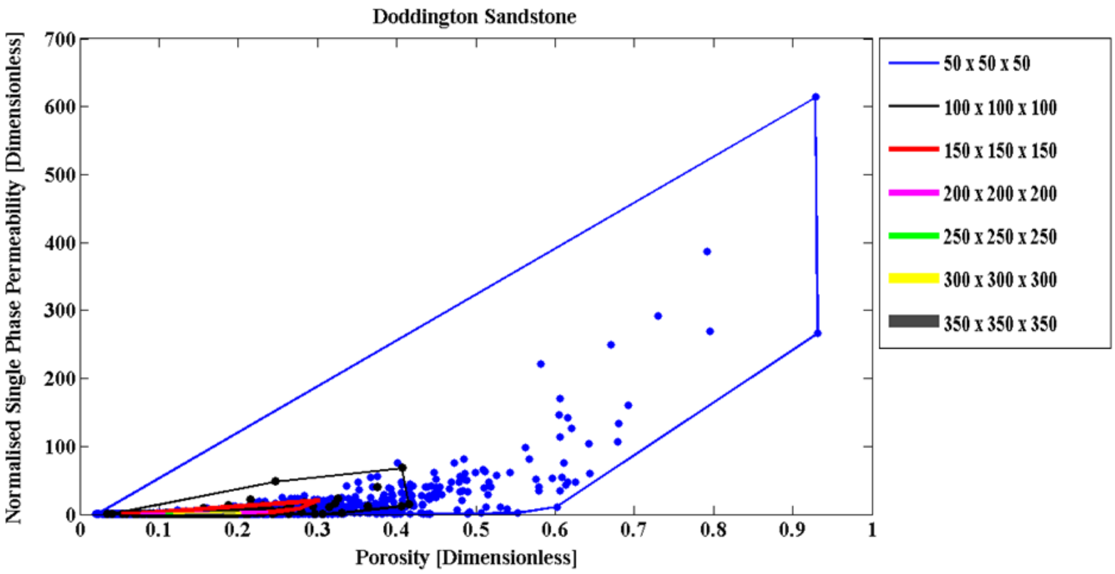

Figure 5. The concept of convex hull applied to the plotted values of porosity and single-phase permeability calculated using LB method for different divided sub-domains varying from 50^3 to 350^3 voxels. The data is shown for a Doddington sandstone sample.

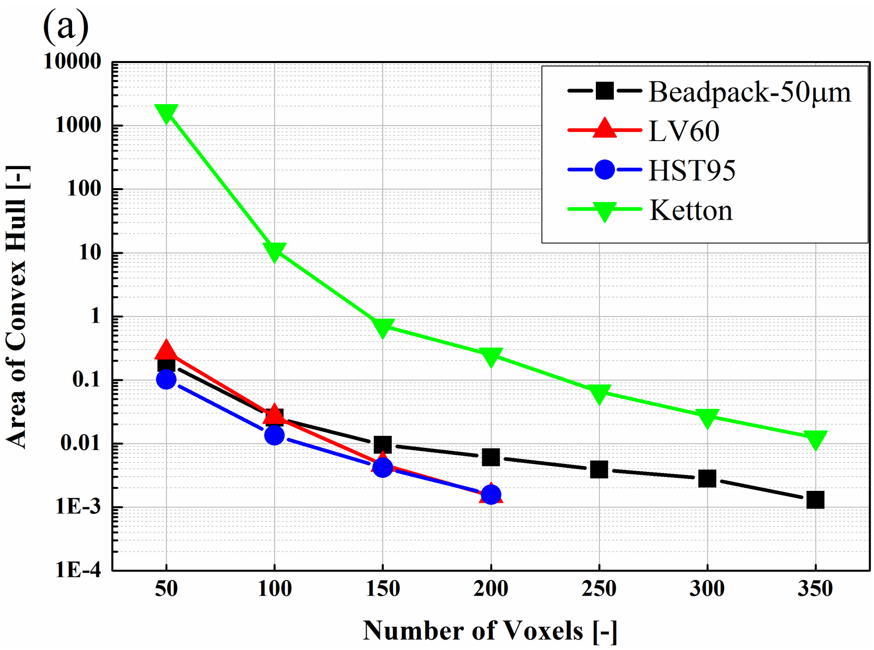

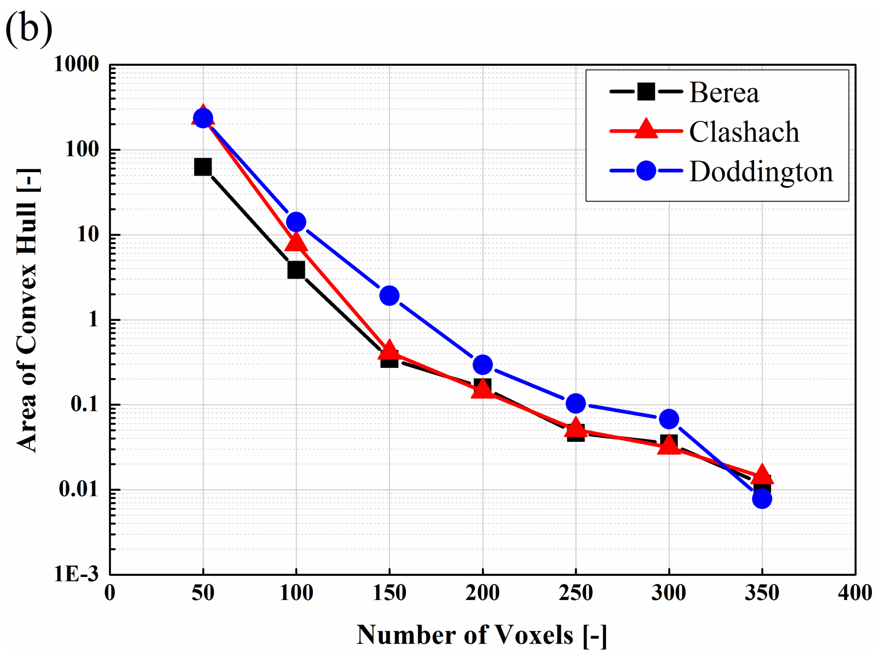

Figure 6. The calculated area of convex hull for domain sizes ranging from 50^3 to 350^3 voxels is shown for beadpack, sandpacks and carbonate in figure (a), for sandstones in figure (b). The REV size for each sample can be determined by choosing an acceptable area for the convex hull, for example 0.5 will be used here, and reading the corresponding system size.

From Figures 5 and 6, we observe that the area of the convex hull systematically decreases as the size of the sub-domain increases from 50^3 to 350^3 voxels for each of the rock types. The REV is then estimated by choosing a value of the area of the convex hull area below which the variations of both parameters are acceptable, for example 0.5. We note that one limitation of this approach is that the hull area cannot be simply related to statistical measures such as the variance of the individual parameters, so the choice of threshold is somewhat arbitrary. From figures 6 (a) and (b) we can then determine the REV size for beadpacks, sandpacks, sandstones and carbonate rock types. The beadpacks and the two sandpacks samples, LV60 and HST95, converge faster than sandstones and carbonate needs only a sub-domain greater than 50^3 voxels (or 250 µm in linear dimensions). Using the same hull area threshold of 0.5, the REV size for Berea and Clashach sandstone comes to 150^3 voxels (750µm), while for Doddington it is somewhat larger, around 200^3 voxels (904µm). The REV size for Ketton is greater than 150^3 voxels (750µm).

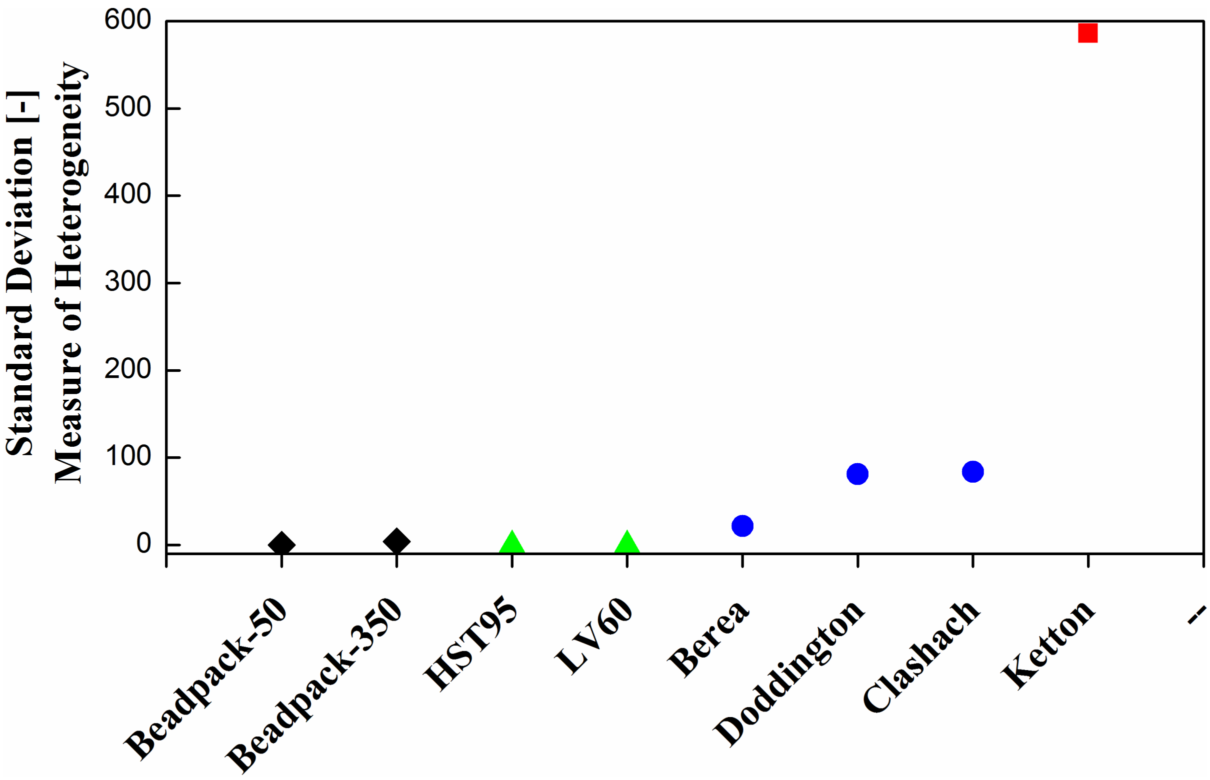

Figure 7. Standard deviation values for the calculated convex hull area for each rock sample as a function of measure of heterogeneity. Black indicates beadpacks, green indicates sandpacks, blue indicates sandstones and red indicate carbonate samples.

Another quantitative measure of heterogeneity is defined here as the standard deviation of the calculated area of the convex polygon for the entire sub-divided domain varying from 50^3 to 350^3 voxels. Figure 7 shows this measure of heterogeneity for the entire library of rocks used in this study. Comparing the standard deviations, to understand the heterogeneity of the rock across the whole domain of 700^3 voxels, we observe that the calculated values of the standard deviation are very small and constant for beadpacks and two sandpacks, LV60 and HST 95. For beadpacks and sandpacks, the calculated standard deviations vary within a small range, whereas sandstone and carbonate rocks show a significant variation in the calculated standard deviation for different rock samples indicating the heterogeneity across the whole domain of 700^3 voxels.

The REV sizes determined above suggest that we can capture a typical length scale of heterogeneity. However, this estimated REV size, although useful to estimate the size of simulation required for parameter estimation, does not allow a satisfactory ranking of sample heterogeneity. To illustrate this issue, consider two bead packs, of different grain size that are otherwise identical, as shown in Figure 8. The permeability/porosity convex hull areas of the two bead packs, shown in Figure 9, are very different, but intuitively both are equally homogeneous. Hence, there is a need to introduce a new scaling factor for sub-domain or voxel size to optimize the convex hull process to obtain a more satisfying description of the heterogeneity.

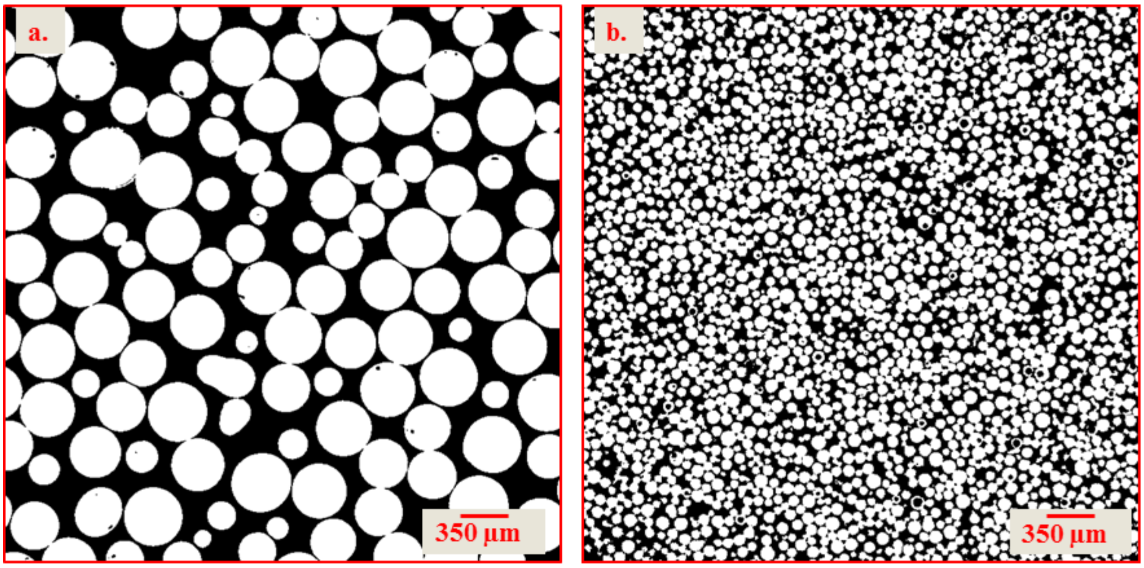

Figure 8. Binarized two-dimensional cross-sections of the three dimensional data set of Bead packs with (a) Grain size = 350µm and (b) Grain size = 50µm respectively. White colour represents the grain space and black colour indicates the pore space

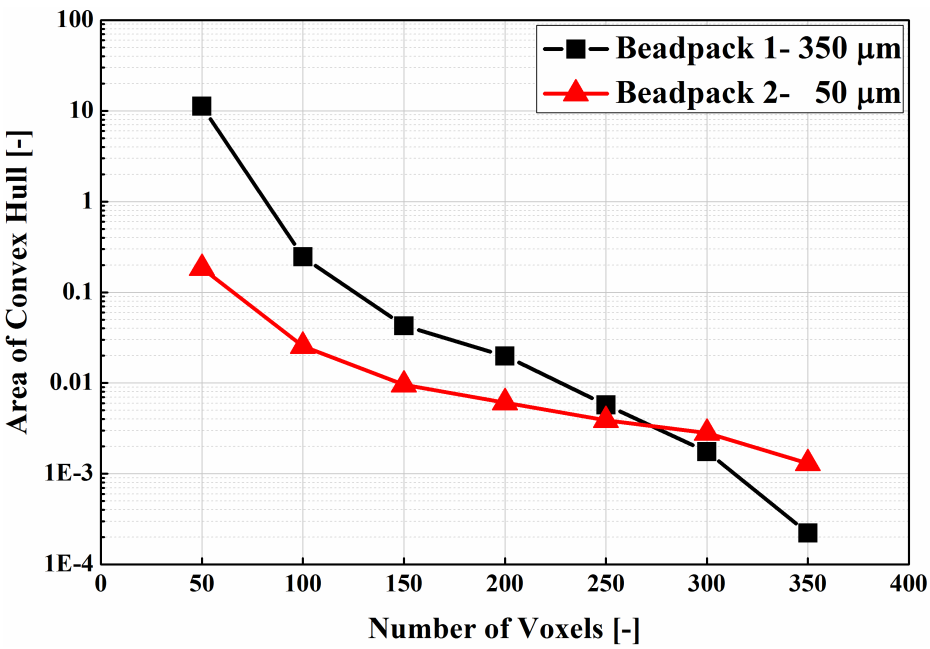

Figure 9. Calculated area of convex hull for voxel sizes ranging from 50^3 to 350^3 is shown for two bead packs with grain sizes 350µm and 50µm.

The origin of the characteristic length is open to choice and the grain size is commonly used in the literature (Kameda & Dvorkin, 2004). However, while this may be appropriate for estimation of mechanical properties, the average pore diameter is a more natural choice for fluid flow parameters. The average pore diameter for all the samples was estimated using the maximum ball algorithm approach where spheres are grown in the pore space of segmented 3D micro-CT data, centred on each pore voxel (Dong & Blunt, 2009). Table 4 shows the calculated mean pore size for the library of rock images used in this study.

Table 4 Mean pore size for all samples estimated by the maximum ball algorithm.

Sample	Mean Pore Size (µm)
Beadpack – 50 µm	20.02
Beadpack – 350 µm	56.44
LV60 sandpack	47.5
HST95 sandpack	34.76
Berea sandstone	20.98
Clashach sandstone	34.92
Doddington sandstone	37.18
Ketton carbonate	57.18

We have scaled the sub-domain sizes for all the samples by the corresponding mean pore size and Figure 10 shows the convex hull areas plotted against the resulting dimensionless length. The scaling resolves several issues in the comparison of relative heterogeneity. In the earlier analysis Ketton, a well-sorted oolitic limestone with almost spherical grains, appeared more heterogeneous than the sandstones, whereas Figure 10 shows that this was mostly due to the large pore size of Ketton which now falls close to the group of sandpacks.

Figure 10 also shows that simply relating the REV to pore size is insufficient as the data do not collapse onto a master curve now system size is scaled by pore size. Keeping our choice of acceptable hull area at 0.5, only Clashach and Doddington fall close to the L = 20a relationship proposed by Keehm (Keehm, 2003). The beadpacks and sandpacks, on the other hand, reach the threshold around 10a and Ketton carbonate around 12a. The more complex Berea sandstone requires around 35a.

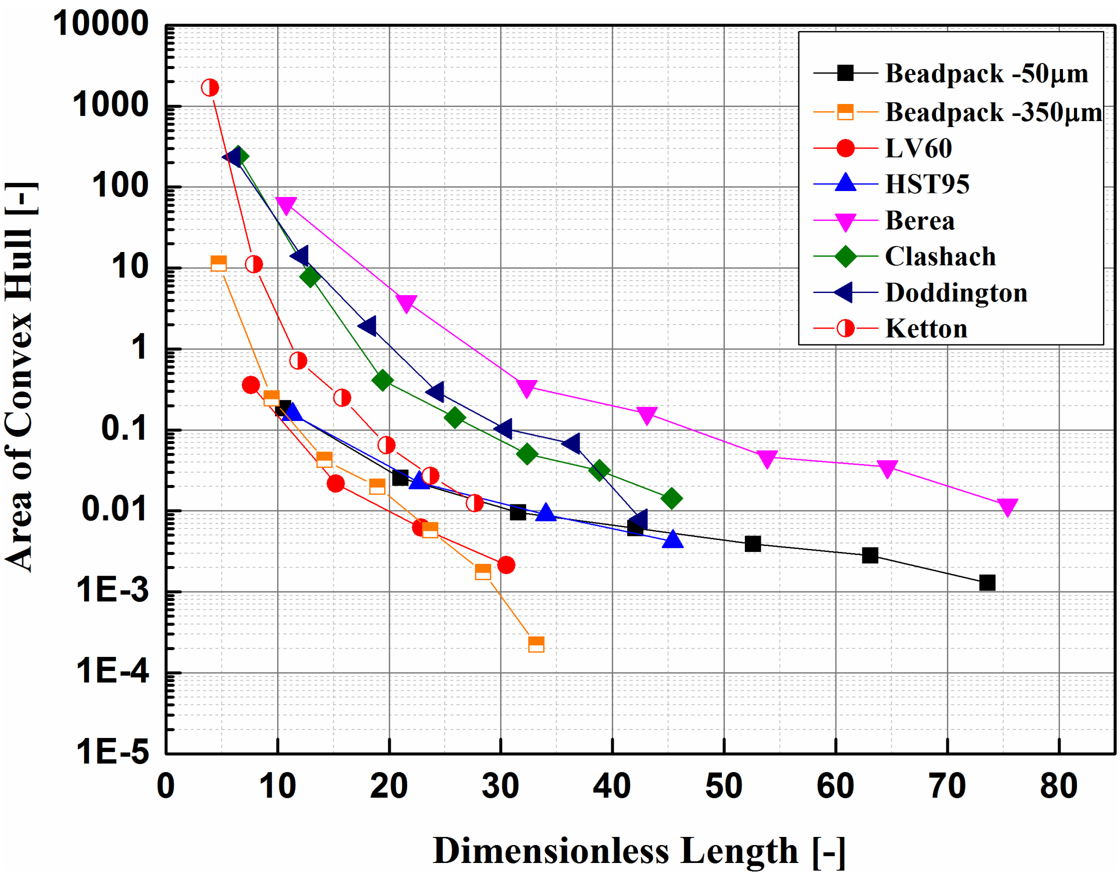

Figure 10. Porosity/permeability convex area against dimensionless for the entire rock library.

In the examples above, the permeability ranges over several orders of magnitude. Consequently the variance to small permeability has little impact on the area of the convex hull, as can be seen in Figure 5 where the shape of the hull becomes rather linear as the system size is increased. A more evenly weighted convex hull can be made when the log of the permeability is taken first for each of the sub-sampled system sizes and then normalised with respect to the log of the permeability calculated from the largest system size. This is shown, again for the Doddington sandstone, in Figure 11 where the hull retains its two-dimensional shape at intermediate system sizes.

Note that there is evidence for a correlation between permeability and porosity in figure 11, as the hull for the 50µm bead pack in particular tends towards a line with a finite slope at large system size. The use of such correlations, for example the Carman-Kozeny equation, for estimating the permeability of complex rocks from the correlation between permeability and porosity has been discussed in the literature, see for example Mostaghimi et al. (2013). The main issue being that the Kozeny constant can take a wide range of values depending on the rock structure. Here the main emphasis is on estimating the REV rather than comparing methods for estimating the permeability. In this case the porosity and permeability converge at a similar rate, as the hull would tend towards either a vertical or horizontal line if one variable reached a stationary value before the other as the system size was increased. This implies that the REV for permeability and porosity are similar in the Beadpack-50μm sample and there is strong correlation between porosity and permeability. However this behaviour was not universal and a non-linear hull is persistent, particularly for the sandpacks

The convex hull approach would not be appropriate for rocks in which the parameters converged to their REV values at very different rates. In this case one parameter would come to dominate the variation and the hull would appear as a horizontal or vertical line, however this was not the case for any of the examples shown here.

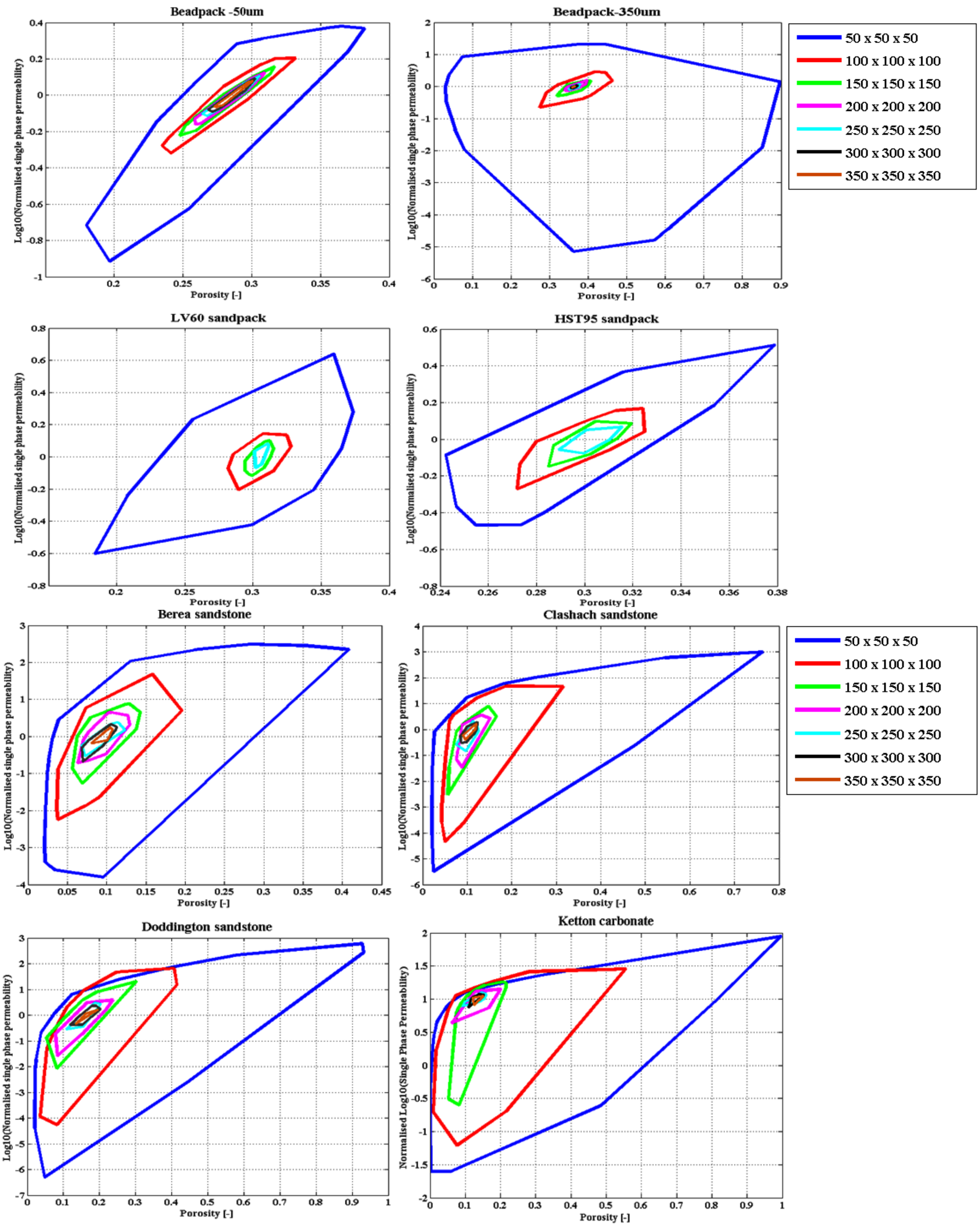

Figure 11. Convex hull of Log_{10} (K) against porosity. (a) Beadpack 50 µm. (b) Beadpack 350 µm. (c) HST95 sandpack (d) LV60 sandpack (e) Berea sandstone (f) Clashach sandstone (g) Doddington sandstone (h) Ketton carbonate.

Interestingly, plotting the convex hull area of the log(k), porosity space against the dimensionless length, improves the exponential decay fit as is shown in Figure 12 (a) for beadpacks, sandpacks, carbonate and Figure 12 (b) for sandstones rocks respectively. They are all linear on a log (area of convex hull) – linear (length) graph. This suggest a further gain in computational efficiency to be made by only computing the parameters for small system sizes and using the resulting exponential to extrapolate REV. Table 5 shows the predicted exponential decay constant and the pre-factor predicted from the exponential decay fit to obtain quantitative data for all the rocks studied using

$$A = ae^{kl}, (k < 0) \qquad (1)$$

where,

A = Convex hull area

a = Exponential pre-factor constant

k = Exponential decay constant

l = dimensionless length

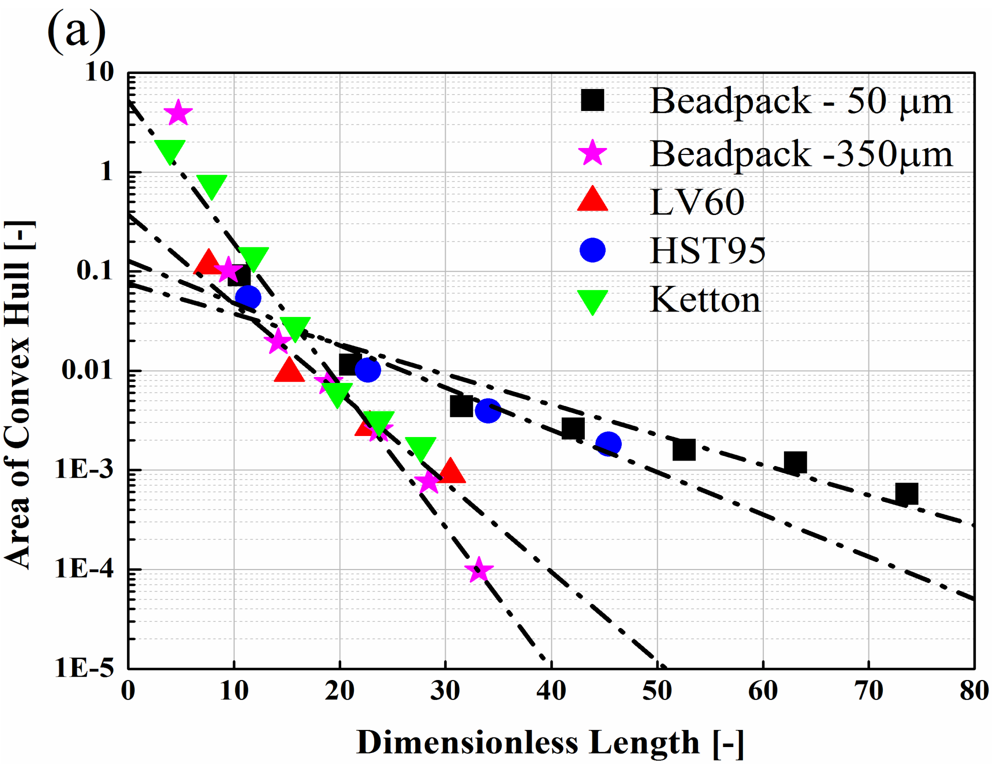

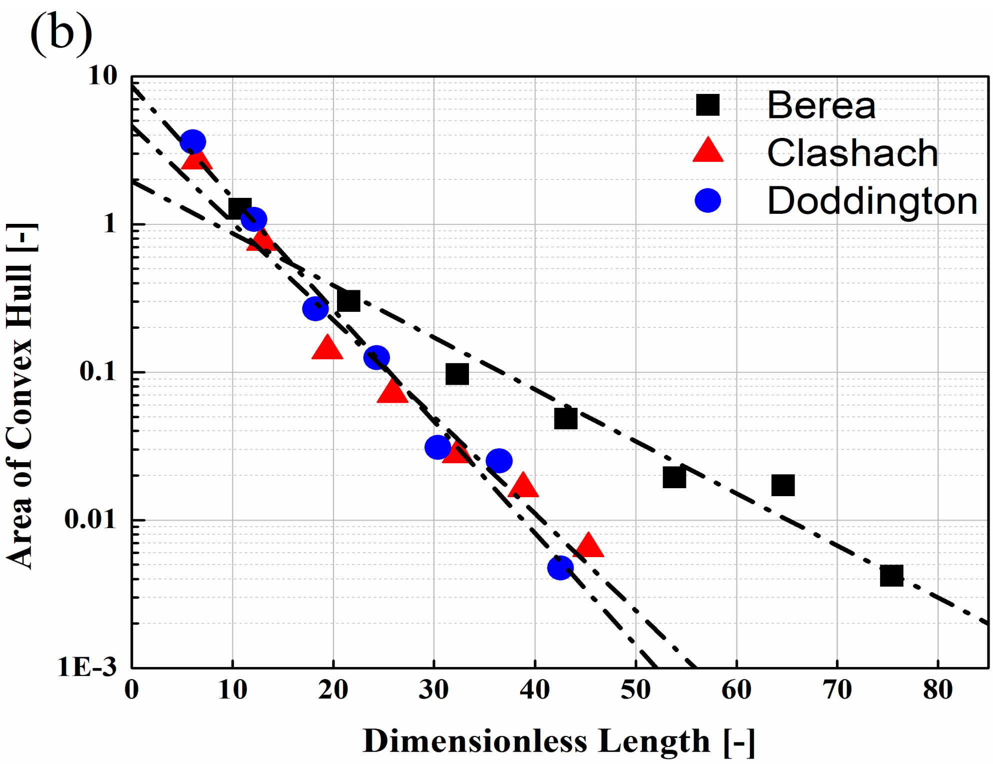

Figure 12. Logarithmic area of convex hull showing exponential decay (dash line, black colour) when plotted against dimensionless length. (a) Beadpacks, sandpacks and carbonate samples. (b) Sandstone samples.

Table 5 Predicted exponential pre-factor and decay constant for the different rocks studied.

Sample	Exponential pre-factor constant	Exponential decay constant	R^2
Beadpack-50µm	0.0752	-0.07	0.8966
Beadpack-350µm	5.164	-0.329	0.9512
LV60 sandpack	0.3725	-0.207	0.9575
HST95 sandpack	0.128	-0.098	0.9656
Berea sandstone	1.95	-0.081	0.968
Clashach sandstone	4.6473	-0.151	0.9721
Doddington sandstone	8.5826	-0.174	0.984
Ketton carbonate	5.8244	-0.314	0.9754

The values of the exponential pre-factor and decay constant in Table 4 show a systematic trend for the different rocks studied. The decay constant for Berea is -0.08 and about -0.17 for Doddington sandstone. This means that the decay is slower for a heterogenous rock (Berea) than for a relatively homogenous rock (Doddington and Clashach). This in turn suggests that a critical value of the REV is reached more quickly (at smaller dimensionless length) for homogenous than for more heterogenous sandstones. This is what we expect qualitatively (see Figure 10), but now we can quantify this for different rocks by providing the value of the decay exponent and the pre-factor from the exponential fit.

5. Conclusions

We quantified the degree of heterogeneity for different rock images by sampling the porosity and permeability at different sub-volume sizes and using the convex hull concept. In the past, the REV size was determined from individual macroscopic properties such as porosity, permeability and specific surface area, but here we are computing an REV size based on two parameters combined. By scaling the volume dimension with an average pore-diameter, a quantitative measure of REV size was obtained from the convergence behaviour of the convex hull area as the volume considered increased. It was found that this convergence behaviour can be extrapolated from a few data points from small sub-volume sizes on a logarithmic scale, potentially reducing the computational workload required in REV determination with this method. The convex hull technique can in principle be extended to include further macroscopic properties, and this will be investigated in future studies.

Acknowledgements

This work was carried out as part of the activities of the Qatar Carbonates & Carbon Storage Research Centre (QCCSRC) at Imperial College London. We gratefully acknowledge the funding of QCCSRC provided jointly by Qatar Petroleum, Shell, and the Qatar Science and Technology Park, and their permission to publish this research. S.Shah is grateful to BG Group for funding his PhD project through Imperial College Centre for CCS. Kamaljit Singh (Department of Earth Science and Engineering, Imperial College London) is gratefully acknowledged for providing micro-CT scans.

References

Al-Raoush, R., & Papadopoulos, A. (2010). Representative elementary volume analysis of porous media using X-ray computed tomography. *Powder Technology, 200*(1-2), 69-77.

Andrew, A. M. (1979). Another efficient algorithm for convex hulls in two dimensions. *Information Processing Letters, 9*(5), 216-219.

Andrew, M., Bijeljic, B., & Blunt, M. J. (2013). Pore-scale imaging of geological carbon dioxide storage under in situ conditions. *Geophysical Research Letters, 40*(15), 3519-3918.

Arns, C. H., Knackstedt, M. A., Pinczewski, W., & Martys, N. S. (2004). Virtual permeametry on microtomographic images. *Journal of Petroleum Science and Engineering, 45*(1-2), 41-46.

Auzerais, F. M., Dunsmuir, J., Ferreol, B. B., Martys, N., Olson, J., Ramakrishnan, T. S., . . . Schwartz, L. M. (1996). Transport in sandstone: A study based on three dimensional microtomography. *Geophysical Research Letters, 23*(7), 705-708.

Bear, J. (1972). *Dynamics of Fluids in Porous Media.* American Elsevier Publishing Company.

Blunt, M. J., Bijeljic, B., Dong, H., Gharbi, O., Iglauer, S., Mostaghimi, P., . . . Petland, C. (2013). Pore-scale imaging and modelling. *Advances in Water Resources, 51*, 197-216.

Blunt, M. J., Jackson, M. D., Piri, M., & Valvatne, P. H. (2002). Detailed Physics, Predictive Capabilities and Macroscopic Consequences for Pore-Network Models of Multiphase Flow. *Advances in Water Resources, 25*(8), 1069-1089.

Boek, E. S., & Venturoli, M. (2010). Lattice-Boltzmann studies of fluid flow in porous media with realistic rock geometries. *Computers and Mathematics with Applications, 59*(7), 2305-2314.

Bosl, W. J., Dvorkin, J., & Amos, N. (1998). A study of porosity and permeability using a lattice Boltzmann simulation. *Geophysical Research Letters, 25*(9), 1475-1478.

Chen, S., Wang, Z., Shan, X., & Doolen, G. D. (1992). Lattice Boltzmann computational fluid dynamics in three dimensions. *Journal of Statistical Physics, 68*(3), 379-400.

Crawshaw, J. P., & Boek, E. S. (2013). Multi-scale Imaging and Simulation of Structure, Flow and Reactive Transport for CO2 Storage and EOR in Carbonate Reservoirs. *Reviews in Mineralogy & Geochemistry, 77*(1), 431-458.

Dong, H., & Blunt, M. J. (2009). Pore-network extraction from micro-computerized tomography images. *Physical Review E 80, 036307*.

Fredrich, J. T. (1999). 3D Imaging of porous media using laser scanning confocal microscopy with application to microscale transport processes. *Physics and Chemistry of the Earth, Part A: Solid Earth and Geodesy, 24*(7), 551-561.

Gray, F., Cen J., Shah, S. M. Crawshaw J.P. and Boek E.S. (2016) Simulating Dispersion in Porous Media and the Influence of Segmentation on Stagnancy in Carbonate *Advances in Water Resources* **97**, 1-10

Kameda , A., & Dvorkin, J. (2004). To see a rock in a grain of sand. *The Leading Edge, 23*(8), 790-792.

Keehm, Y. (2003). *COMPUTATIONAL ROCK PHYSICS: TRANSPORT PROPERTIES.* Stanford University, California. Retrieved from https://pangea.stanford.edu/departments/geophysics/dropbox/SRB/public/docs/theses/SRB_090_JAN03_Keehm.pdf

Knackstedt, M., Christoph, A., Ghous, A., Sakellariou, A., Senden, T., Adrian, S., . . . Ioannidis, M. A. (2006). 3D Imaging and flow characterization of the pore space of carbonate rock samples. *Society of Core Analysts*, (SCA2006-23). Paper presented at the International Symposium of the Society of Core Analysts. Dublin, CA: Society of Core Analysts.

Mostaghimi, P., Blunt, M. J., & Branko, B. (2013). Computations of Absolute Permeability on Micro-CT Images. *Mathematical Geosciences, 45*(1), 103-125.

Nordahl, K., & Ringrose, P. S. (2008). Identifying the Representative Elementary Volume for Permeability in Heterolithic Deposits Using Numerical Rock Models. *Mathematical Geosciences, 40*, 753-771.

Olea, R. A. (Ed.). (1991). *Geostatistical Glossary and Multilingual Dictionary.* New York: Oxford University Press.

Pan, C., Hilpert, M., & Miller, C. T. (2001). Pore-scale modeling of saturated permeabilities in random sphere packings. *Physical Review E 64, 066702*.

Peng, S., Hu, Q., Dultz, S., & Zhang, M. (2012). Using X-ray computed tomography in pore structure characterization for Berea sandstone: resolution effect. *Journal of Hydrology, 472-473*, 254-261.

Peng, S., Marone, F., & Dultz, S. (2014). Resolution effect in X-ray microcomputed tomography imaging and small pore's contribution to permeability for a Berea sandstone. *Journal of Hydrology, 510*, 403-411.

Shah, S. M., Crawshaw, J. P., & Boek, E. S. (2016). Micro-Computed Tomography Pore-scale Study of Flow in Porous Media:Effect of Voxel Resolution. *Advances in Water*

Resources, 95(Special issue in Advances in Water Resources: Pore-scale modeling and experiments), 276-287.

Shah, S. M., Crawshaw, J. P., & Boek, E. S. (2016). Three-dimensional imaging of porous media using confocal laser scanning microscopy. *Journal of Microscopy*.

Shah, S. M., Yang, J., Crawshaw, J. P., Gharbi, O., & Boek, E. S. (2013). Predicting Porosity and Permeability of Carbonate Rocks From Core-Scale to Pore-Scale Using Medical CT, Confocal Laser Scanning Microscopy and Micro CT. *SPE 166252.* New Orleans, Louisiana, USA.

Spanne, P., Thovert, J. F., Jacquin, C. J., Lindquist, W. B., Jones, K. W., & Adler, P. M. (1994). Synchrotron computed microtomography of porous media - Topology and Transports. *Physical Review Letters, 73*(14), 2001-2004.

Valvatne, P. H., & Blunt, M. J. (2004). Predictive pore-scale modeling of two-phase flow in mixed wet. *Water Resources Research, 40*(W07406).

Walsh, J. B., & Brace, W. F. (1984). The effect of pressure on porosity and the transport properties of rock. *Journal of Geophysical Research: Solid Earth, 89*(B11), 9425-9431.

Yang, J., & Boek, E. S. (2013). A comparison study of multi-component Lattice Boltzmann models for flow in porous media applications. *Computers & Mathematics with Applications, 65*(6), 882-890.

Yang, J., Crawshaw, J. P., & Boek, E. S. (2013). Quantitative determination of molecular propagator distributions for solute transport in homogeneous and heterogeneous porous media using lattice Boltzmann simulations. *Water Resources Research, 49*(12), 8531-8538.

Zhang, D., Zhang, R., Chen, S., & Soll, W. E. (2000). Pore-scale study of flow in porous media: Scale dependency, REV, and statistical REV. *Geophysical Research Letters, 27*(8), 1195-1198.